## Genetically Encoded Lizard Color Divergence for Camouflage and Thermoregulation

Bao-Jun Sun (1), 1,† Wei-Ming Li, 1,† Peng Lv, 2,3,† Guan-Nan Wen, 1,† Dan-Yang Wu, 1 Shi-Ang Tao, 1 Ming-Ling Liao (1), Chang-Qing Yu, Zhong-Wen Jiang, Yang Wang, Hong-Xin Xie, Xi-Feng Wang, Zhi-Qiang Chen, Feng Liu , 2,\* and Wei-Guo Du 11.\*

Associate editor: Sandro Bonatto

#### **Abstract**

Local adaptation is critical in speciation and evolution, yet comprehensive studies on proximate and ultimate causes of local adaptation are generally scarce. Here, we integrated field ecological experiments, genome sequencing, and genetic verification to demonstrate both driving forces and molecular mechanisms governing local adaptation of body coloration in a lizard from the Qinghai-Tibet Plateau. We found dark lizards from the cold meadow population had lower spectrum reflectance but higher melanin contents than light counterparts from the warm dune population. Additionally, the colorations of both dark and light lizards facilitated the camouflage and thermoregulation in their respective microhabitat simultaneously. More importantly, by genome resequencing analysis, we detected a novel mutation in Tyrp1 that underpinned this color adaptation. The allele frequencies at the site of SNP 459# in the gene of Tyrp1 are 22.22% G/C and 77.78% C/C in dark lizards and 100% G/G in light lizards. Model-predicted structure and catalytic activity showed that this mutation increased structure flexibility and catalytic activity in enzyme TYRP1, and thereby facilitated the generation of eumelanin in dark lizards. The function of the mutation in Tyrp1 was further verified by more melanin contents and darker coloration detected in the zebrafish injected with the genotype of Tyrp1 from dark lizards. Therefore, our study demonstrates that a novel mutation of a major melanin-generating gene underpins skin color variation co-selected by camouflage and thermoregulation in a lizard. The resulting strong selection may reinforce adaptive genetic divergence and enable the persistence of adjacent populations with distinct body coloration.

Key words: color polymorphism, ecological adaptation, camouflage, thermal melanism hypothesis, melanin, reptile.

## Introduction

Divergent selection maintains adaptive divergence between conspecific groups that occupy a heterogeneous environment and may lead to local adaptation (Hendry et al. 2009; White and Butlin 2021). In nature, species may experience multiple biotic and abiotic stresses that drive local adaptation. However, how species respond to these kinds of selective pressures phenotypically and genetically remains elusive. To answer these questions, we not only need to identify the role of these selective pressures in shaping and maintaining phenotypic divergence, but also need to explore the genetic basis underpinning local adaptation.

Animal body coloration is an important phenotypic trait that can aid our understanding of local adaptation. This is because an animal's body coloration serves multiple functions including camouflage and thermoregulation that affect individual fitness (Clusella-Trullas et al. 2007; Stevens and Merilaita 2009; White and Kemp 2015). Camouflage, which

Received: April 04, 2023. Revised: January 03, 2024. Accepted: January 08, 2024 © The Author(s) 2024. Published by Oxford University Press on behalf of Society for Molecular Biology and Evolution. This is an Open Access article distributed under the terms of the Creative Commons Attribution-NonCommercial License (https:// creativecommons.org/licenses/by-nc/4.0/), which permits non-commercial re-use, distribution, and reproduction in any medium, provided the original work is properly cited. For commercial re-use, please contact journals.permissions@oup.com

**Open Access** 

<sup>&</sup>lt;sup>1</sup>Key Laboratory of Animal Ecology and Conservation Biology, Institute of Zoology, Chinese Academy of Sciences, Beijing 100101. China

<sup>&</sup>lt;sup>2</sup>State Key Laboratory of Membrane Biology, Institute of Zoology, Chinese Academy of Sciences, Beijing 100101, China

<sup>&</sup>lt;sup>3</sup>University of Chinese Academy of Sciences, Beijing 100049, China

 $<sup>^4</sup>$ The Key Laboratory of Mariculture, Ministry of Education, Fisheries College, Ocean University of China, Qingdao 266003, China

<sup>&</sup>lt;sup>5</sup>Ecology Laboratory, Beijing Ecotech Science and Technology Ltd, Beijing 100190, China

<sup>&</sup>lt;sup>6</sup>Kev Laboratory of Animal Physiology, Biochemistry and Molecular Biology of Hebei Province, College of Life Sciences, Hebei Normal University, Shijiazhuang 050024, China

<sup>&</sup>lt;sup>7</sup>Novogene Bioinformatics Institute, Beijing, China

<sup>&</sup>lt;sup>†</sup>These authors contributed equally.

<sup>\*</sup>Corresponding authors: E-mails: duweiguo@ioz.ac.cn; liuf@ioz.ac.cn.

increases the crypsis of animals to their predators and preys, is one of the most crucial functions of body coloration (Stevens and Merilaita 2011). In addition, the coloration also serves thermoregulation. The thermal melanin hypothesis (TMH) suggests that dark individuals heat up faster than light individuals, giving them a thermoregulatory advantage and therefore higher fitness in cooler environments (Clusella-Trullas et al. 2007). Consistent with this hypothesis, body coloration in many ectotherms is lighter in warm regions and darker in cold regions (Clusella-Trullas et al. 2008; Heidrich et al. 2018). However, the dual functions of camouflage and thermoregulation served by body coloration in ectotherms are not always satisfied synchronically in natural populations, which depend on the environmental context and selective pressures (Umbers 2011; Vroonen et al. 2012; Munguia et al. 2013). For instance, the variation of coloration in wild bearded dragons (Pogona vitticeps) and toadheaded agama (Phrynocephalus grumgrzimailoi) primarily improves camouflage due to the pressure of predators, but compromises thermoregulation (Smith et al. 2016; Tao et al. 2018). Therefore, identifying the role of camouflage and thermoregulation in shaping animal body coloration via manipulative ecological experiments is essential to revealing the driving force of local adaptation in body coloration.

In addition to the driving force, the genetic basis of body coloration is critical for understanding the origin and maintenance of local adaptation (Tigano and Friesen 2016). The darkness of body coloration in ectotherms can be determined by pigmental and structural coloration (Stuart-Fox et al. 2021). The most important mechanism underpinning dark coloration is pigment deposition in melanocytes (Aspengren et al. 2009; Stuart-Fox et al. 2021), which selectively absorb light with specific wavelengths, allowing the light of other wavelengths to be reflected and therefore produce colors (Morehouse et al. 2007). The melanocytes produce two types of melanineumelanin and pheomelanin—which results in black to brown, and red to yellow coloration, respectively (Kaelin and Barsh 2013). Accordingly, dark coloration is determined by the types, density, and area of distribution of melanin, which in turn is determined by the melanin synthesis pathway regulated by the Melanocortin-1 receptor (Mc1r) and its second messenger cyclic adenosine monophosphate (cAMP) (Aspengren et al. 2009; Manceau et al. 2010; McNamara et al. 2021). Specifically, the important regulatory genes (e.g. Mc1r, Agouti, Oca2, Tyr, Tyrp1) in the "cAMP pathway" induce differences in melanin generation and determine the darkness of the skin (Steiner et al. 2007; Manceau et al. 2010; Rosenblum et al. 2010; Orteu and Jiggins 2020). Therefore, exploring the "cAMP pathway" can help identify the molecular mechanism underlying body coloration determination, and increase our understanding of how biotic and abiotic environments shape adaptive genetic divergence among species or populations.

Here we studied adjacent populations of the species of toad-headed agama, *Phrynocephalus putjatai*, distributed in two distinct habitats on Qinghai-Tibet Plateau (QTP)— alpine meadows and sand dunes—with two distinct

phenotypes (dark vs. light) in dorsal coloration. By integrating field behavioral experiments, laboratory manipulation, genomic and transcriptomic sequencing, and gene function verification, we identified the functions of dark and light dorsal coloration in camouflage and thermoregulation, and analyzed the physiological and molecular mechanisms underlying the variation in dorsal coloration. By doing so, we aim to comprehensively reveal the proximate and ultimate causes of local adaptation in lizard dorsal coloration.

#### Results

Lizards from three populations inhabiting cold alpine meadow regions had dark dorsal coloration, whereas lizards from another three populations inhabiting the warmer dune regions had light dorsal coloration. Previous studies revealed P. putjatai is mainly distributed around Qinghai Lake (Jin et al. 2014; Hu et al. 2019; Jin and Brown 2019). However, to avoid confusion with the closely related species (e.g. Phrynocephalus vlangalii), we ascertained the six populations of lizards are P. putiatai with a phylogenetic tree of one mitochondrial DNA gene fragment (1,096 bp of ND2, NADH-dehydrogenase subunit II) and exon of one nuclear DNA gene (634 bp of BDNF, brain-derived neurotrophic factor) (Fig. 1). Therefore, the difference in dorsal colorations between cold alpine meadow and warm dune populations were intraspecific variations. We then used one pair of adjacent populations (i.e. D1 vs. L3 in Fig. 1) to compare the functions and underlying mechanisms of dorsal coloration divergence.

#### The Role of Dorsal Coloration in Camouflage

To identify the function of dorsal coloration in camouflage, we quantified the spectral reflectance of lizards and their microhabitats, and the ratio of different colored lizard models being attacked by natural predators. The dorsal reflectance spectra (i.e. colors) of dark and light lizards was closest to the substrate reflectance of their own habitats in the alpine meadows ( $F_{1,16} = 48.477$ , P < 0.0001) and dunes ( $F_{1,12} = 38.555$ , P < 0.0001), respectively (Figs. 1 and 2a, b; supplementary fig. S1, Supplementary Material online). Correspondingly, the dark-lizard models were attacked less often than were light-lizard models in the alpine meadows (8/47 vs. 20/45,  $\chi^2 = 8.17$ , P < 0.01), while the lightlizard models were attacked less often in the dunes (7/44 vs. 17/44,  $\chi^2 = 5.73$ , P < 0.05; Fig. 2c). This result was consistently validated through replicate testing (in the meadow: 6/42 vs. 17/44,  $\chi^2 = 6.50$ , P < 0.05; in the dunes: 5/40 vs. 14/40,  $\chi^2 = 5.59$ , P < 0.05). The dorsal coloration of lizards matched the reflectance spectra of their respective habitat substrates and therefore reduced predation risk to lizards within their own habitat types.

## The Role of Dorsal Coloration in Thermoregulation

To identify the function of dorsal color in thermoregulation, we measured environmental temperatures, field body temperatures, and heating-up rates of lizards.

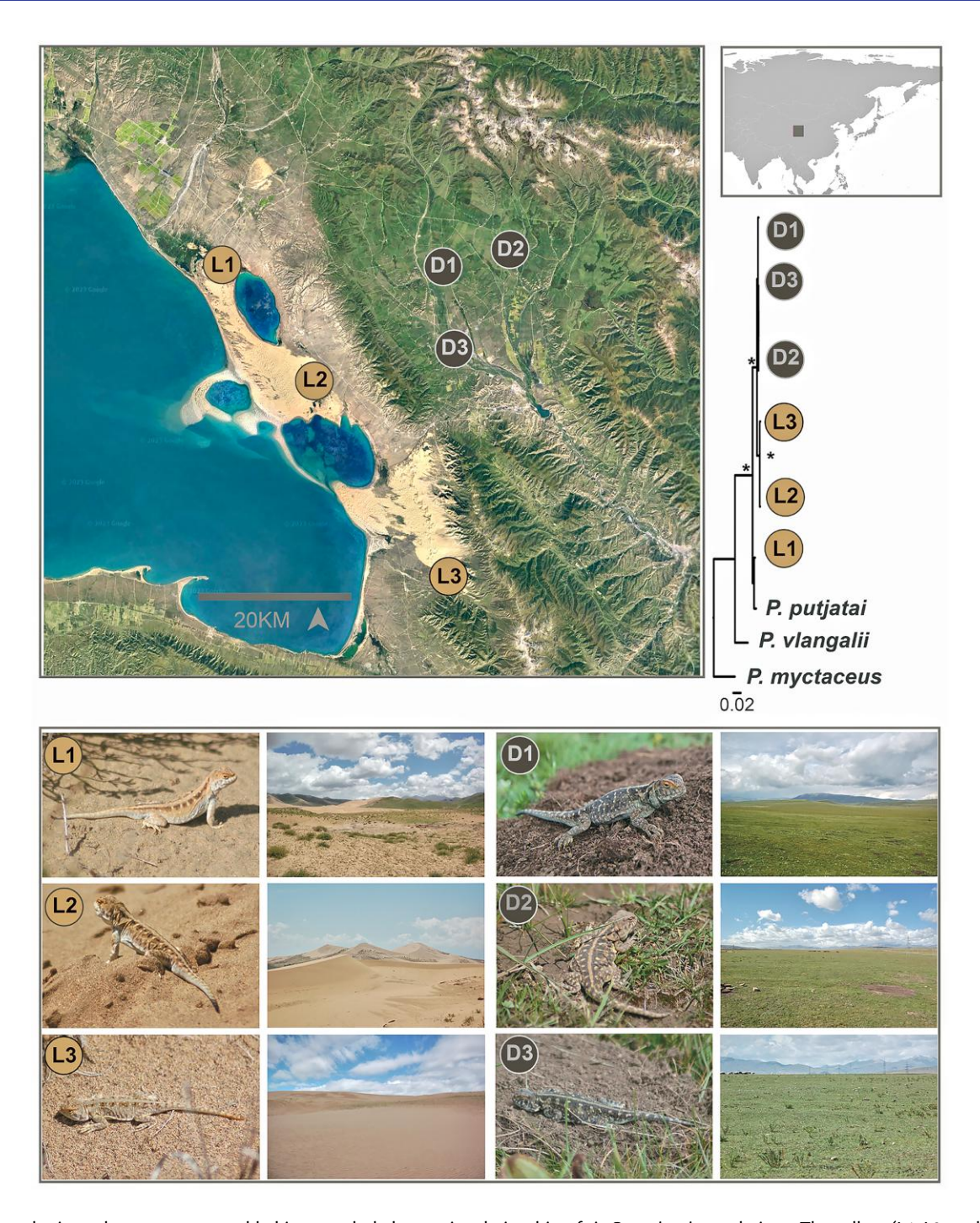


Fig. 1. Sample sites, phenotypes, natural habitats, and phylogenetic relationship of six *P. putjatai* populations. The yellow (L1, L2, and L3) and black (D1, D2, and D3) spots indicate the sample sites of lizards from the dune and alpine meadow habitats, respectively. The photos indicate that the microhabitats for light and dark lizards are significantly different from each other, but are similar to their local microhabitats, respectively. The ML phylogenetic relationship is based on 1,730 bp (partial ND2 and BDNF) sequences. Node strongly supported (BS = 1) is marked with black asterisks. D1 to D3 and L1 to L3 indicate 1 to 3 dark populations (meadow) and 1 to 3 light populations (dune), respectively.

During the lizard activity period from 9 AM to 5 PM, the average surface temperatures ( $T_{\text{surface}}$ ; meadow vs. dune:  $30.56 \pm 0.64$  °C vs.  $35.09 \pm 0.49$  °C;  $F_{1,380} = 31.473$ , P < 0.0001) and air temperatures ( $T_{\text{air}}$ ; meadow vs. dune:  $19.96 \pm 0.34$  °C vs.  $22.54 \pm 0.26$  °C;  $F_{1,380} = 36.066$ , P < 0.0001) were 4.53 and 2.58 °C lower in alpine meadows than in dune habitats, respectively (Fig. 2d and e). However, the average active body temperature ( $T_{\text{b}}$ ) was

only 0.75 °C lower in lizards from the alpine meadow population  $(34.97 \pm 0.21 \,^{\circ}\text{C})$  than in lizards from the dune population  $(35.72 \pm 0.16 \,^{\circ}\text{C}; F_{1,380} = 7.856, P = 0.005; Fig. 2d and e)$ . In addition, the active temperatures of lizards are time-dependent, and the active body temperatures were lower at 9 AM and 5 PM than those from 10 AM to 4 PM  $(F_{8,380} = 13.034, P < 0.001)$ . The heating-up rate was significantly higher for dark alpine

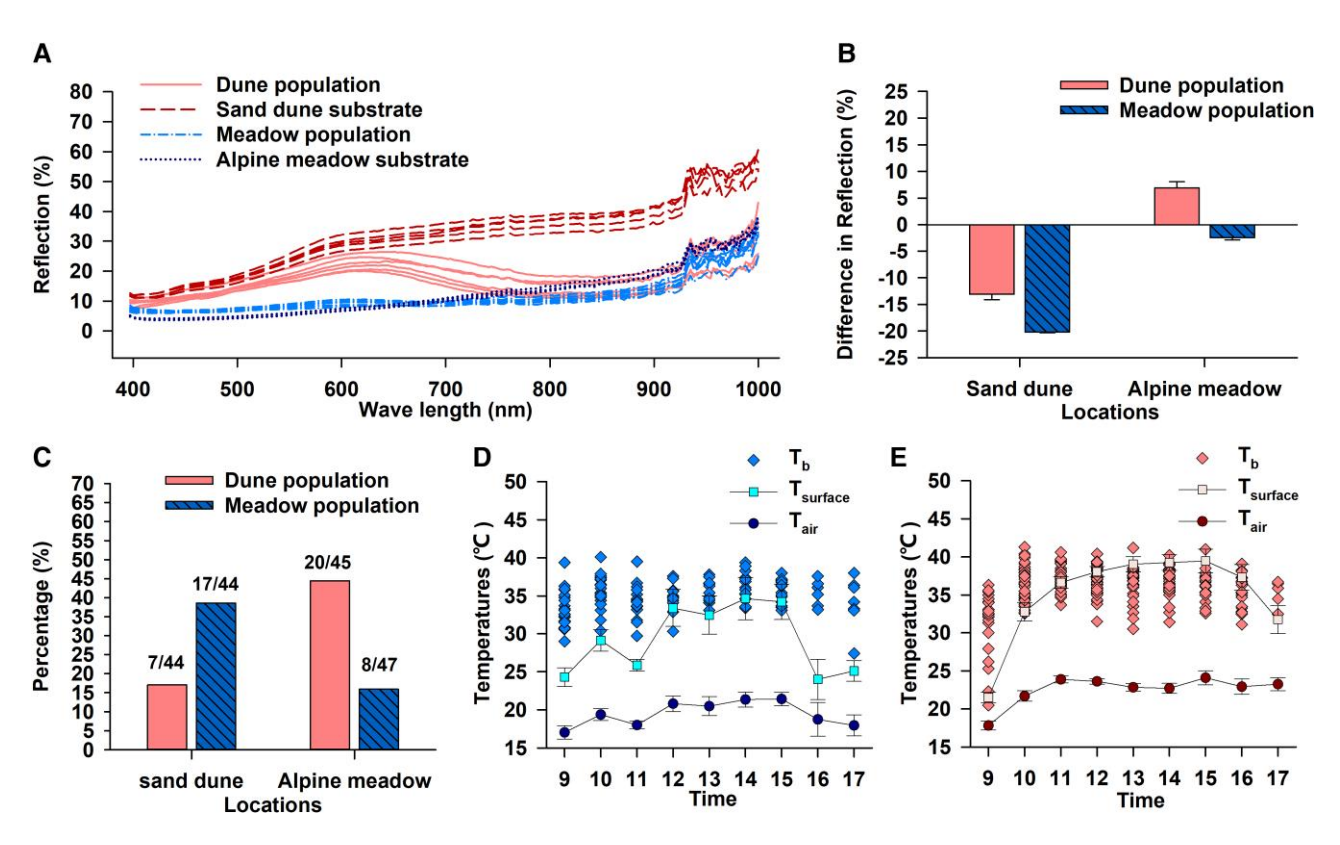


Fig. 2. Functional determination of camouflage and thermoregulation in lizards from the dune and alpine meadow populations with different dorsal coloration. a) Reflectance spectra of the natural substrate and dorsal skin of lizards from the dune and meadow populations under natural light in the field. Each line indicates an individual or a natural substrate in the field. b) The difference in reflectance spectra between the natural substrate and dorsal skin of lizards from the dune and alpine meadow populations. Data are shown as mean  $\pm$  se. (c) The percentage of lizards attacked by avian and mammalian predators in dune and alpine meadow habitats, respectively. Numbers above the columns indicate the sample size of attacked models against the initial set. d, e) Substrate surface temperatures ( $T_{\text{surface}}$ ), air temperatures ( $T_{\text{air}}$ ), and active body temperatures of lizards ( $T_{\text{b}}$ ) in natural habitats of alpine meadow and dune. Each diamond indicates a  $T_{\text{b}}$  from an active individual, and  $T_{\text{surface}}$  and  $T_{\text{air}}$  are shown as mean  $\pm$  se.

meadow lizards than light dune lizards, both in terms of the thermal time constant ( $\tau$ ) from 15 to 30 °C (meadow vs. dune, 379.3  $\pm$  14.5 S vs. 580.3  $\pm$  13.5 S;  $F_{1,29} = 83.446$ , P < 0.0001; supplementary fig. S2a, Supplementary Material online) and the increase in body temperature after 5 min of heating (meadow vs. dune,  $14.36 \pm 0.30$  °C vs.  $10.25 \pm 0.27$  °C;  $F_{1,29} = 84.399$ , P < 0.0001; supplementary fig. S2a, Supplementary Material online). Therefore, compared with the light dorsal coloration of lizards from the warm dune environment, the dark dorsal coloration may help lizards heat up faster and achieve optimal body temperatures in the cold alpine meadow environment.

#### Melanin Abundance in the Dorsal Skin of Lizards

To explore the physiological basis of between-population variation in body color, we compared the difference in abundance of melanin and the metabolites of dorsal skin between the alpine meadow and dune populations. The dorsal skin of lizards from the alpine meadow population had greater surficial areas of melanin ( $F_{1,25} = 11.283$ , P = 0.003; supplementary fig. S3, a and b, Supplementary Material online), higher eumelanin content ( $F_{1,18} = 6.239$ , P = 0.022) and total melanin ( $F_{1,18} = 19.466$ , P = 0.0003) than

those from the dune population (supplementary fig. S3c, Supplementary Material online). In addition, the lizards from the alpine meadow population had a higher abundance of melanin precursors (i.e. Dopa) of L-domachromate (Z = 2.012, P = 0.044) and D-dopachrome (Z = 4.500, P < 0.0001), but not L-dopachrome (Z = 1.353, P = 0.176) than lizards from the dune population (supplementary fig. S3d, Supplementary Material online). Overall, dark lizards from the alpine meadow population had a higher content of melanin and its precursors than light lizards from the dune population.

# Genomic Variation in the Melanin-generating Pathway

To explore the molecular mechanisms of body color variation between the alpine meadow and dune populations, we conducted whole-genome resequencing and transcriptomic sequencing of dark and light lizards. First, our analysis of population structure and demographic history indicated that the adjacent alpine meadow and dune populations had a clear delimitation with a  $F_{ST}$  value of 0.14, revealed by PCA (Fig. 3a) and Admixture (Fig. 3b) based on whole-genome resequencing data. Demographic modeling suggests the initial divergence between alpine meadow and dune

populations happened ~0.26 million years ago (Ma, estimated with 2 yr/generation), and a recent migration ~8,000 years ago, with very unidirectional gene flow from the alpine meadow to the dune population (supplementary fig. S4, Supplementary Material online). Second, we identified 514 outlier candidate genes in the alpine meadow population using an XP-EHH threshold of 1.61879 (i.e. top 5%) (Fig. 3c, supplementary table S1, Supplementary Material online). We discovered a melaningenerating related gene, Tyrp1, attained the highest rank (289th) among all outlier candidate genes associated with melanin generation. This positioned Tyrp1 as the sole melanin-related gene within the top 5% of all outliers (see supplementary table \$1, Supplementary Material online for outliers with the top 5% highest XP-EHH values). In contrast, 288 genes exhibited greater divergence than Tyrp1, as evidenced by higher XP-EHH values. Subsequent Gene Ontology (GO) enrichment analysis highlighted the significant association of these 288 genes with four GO terms: actin-myosin filament sliding, actin-mediated cell contraction, actomyosin structure organization, and muscle filament sliding. Moreover, Tyrp1 displayed a notable difference in allele frequency between the alpine meadow and dune populations at a nonsynonymous polymorphic site (SNP 459; Fig. 3c). We also identified nonsynonymous mutations in other melanin-generating related genes, including Zeb2, Rab1a, Bnc2, and Prep. However, the XP-EHH values for these genes fell below 1.61879, indicating they did not rank within the top 5% (Fig. 3c; supplementary table \$1, Supplementary Material online).

Genomic resequencing indicated that the genotype of Tyrp1 showed a significant differentiation between alpine meadow and dune populations (G/G frequency:  $\chi^2$  = 28.00, P < 0.01), with 22.22% of G/C (2/9) and 77.78% of C/C (7/9) at SNP 459 in the alpine meadow population, but 100% of G/G (19/19) in the dune population (Fig. 3d). Additional Tyrp1 sequencing by PCRs experiment with 30 individuals from each of meadow and dune populations verified the difference in allele frequency (G/G frequency:  $\chi^2 = 34.74$ , P < 0.01), with 40% of G/C (12/30), 33.3% of C/C (10/30), and 26.7% of G/G (8/30) at SNP 459 in lizards from the alpine meadow population, but 100% of G/G (30/30) in lizards from the dune population. Combined the results from both genomic resequencing and PCRs experiment, Tyrp1 exhibited a significant difference in allele frequency between the alpine meadow and dune populations (G/G frequency:  $\chi^2 = 60.13$ , P < 0.01), with 35.90% of G/C (14/39) and 43.59% of C/C (17/39) and 20.51% of G/G (8/39) at SNP 459 in the alpine meadow population. In contrast, the dune population showed 100% G/G (49/49) frequency.

Furthermore, transcriptome sequencing revealed that the expression (Fragments Per Kilobase of exon model per Million mapped fragments: FPKM) of *Tyrp1* gene was significantly higher in the skin of lizards from the alpine meadow population than in those from the dune population. In contrast, other identified melanin-generating

related genes of Zeb2, Rab1a, Bnc2, and Prep, did not show difference in expression between the alpine meadow and dune populations (Fig. 3e). Thus, we infer that the gene Tyrp1 is a primary candidate gene for generating more melanin in dark lizards from the alpine meadow population.

#### Structure and Catalytic Activity of TYRP1

Based on the sequences of the enzyme TYRP1, we predicted the 3-D structure and the catalytic activities of the candidate enzymes by mathematical models. We found that only one mutation out of 1,602 bp, located in the beta-sheet at 459#, induced the amino acid of serine (Ser) in the dune population, but threonine (Thr) in the alpine meadow population (Fig. 3f). Integrative modeling further predicted that the C-score for Ser-459# and Thr-459# were both -1.42, indicating the prediction was reliable. Ser-459# from light lizards had higher numbers of salt bridges and hydrogen bonds, and greater radius of gyration and solvent-accessible surface area than Thr-459# from dark lizards, suggesting more flexibility in the TYRP1 enzyme with Thr-459# (Table 1, supplementary tables S2 and S3. Supplementary Material online). The predicted catalytic activity (K<sub>M</sub>) value for the TYRP1 enzyme with Thr-459# from the alpine meadow population (0.0385) is lower than  $K_{M}$ with Ser-459# from the dune population (0.0442) and other lizard species with light dorsal coloration (supplementary table S4, Supplementary Material online). This indicates higher catalytic activity of TYRP1 from the alpine meadow population, as a lower  $K_{\rm M}$  value means higher catalytic activity.

# Tyrp1<sup>459Thr</sup> Leads to More Melanin Generation in Zebrafish

To verify whether the mutations of the candidate gene can cause changes in skin darkness, we conducted molecular manipulations in a model system of zebrafish. The enzyme of TYRP1 mediates the last step of melanin synthesis by onestep oxidizing DHICA to produce 5,6-IQCA, which is an isoform of melanin (Ito and Wakamatsu 2008) (Fig. 4a). To further confirm the distinct catalytic activity of TYRP1 from Tyrp1<sup>459ser</sup> (light) and Tyrp1<sup>459Thr</sup> (dark) of P. putjatai, we cloned these two types of Flag-tagged *Tyrp1* coding sequence (CDs) of *P. putjatai, Tyrp1* and *Tyrp1* and *Tyrp1* 1376C, into pCS2+ vectors. First, the difference of cloned sequences at 1,376 base was validated by sequencing (Fig. 4b). We then found that both types of Tyrp1 mRNA could be significantly over-expressed (OE) in zebrafish embryos at 36 hpf (i.e. hours post-fertilization) (Fig. 4c and d). Subsequently, we observed that more melanin was synthesized in both Tyrp1 mRNA-injected embryos compared to wild type (WT) at 36 hpf and 4 dpf (i.e. days post-fertilization) (Fig. 4e; supplementary fig. S5, a to c, Supplementary Material online). The number of melanocytes did not differ between WT and both Tyrp1 OE groups at 36 hpf (supplementary fig. S5d, Supplementary Material online). However, the surficial areas of dorsal melanin significantly increased in both

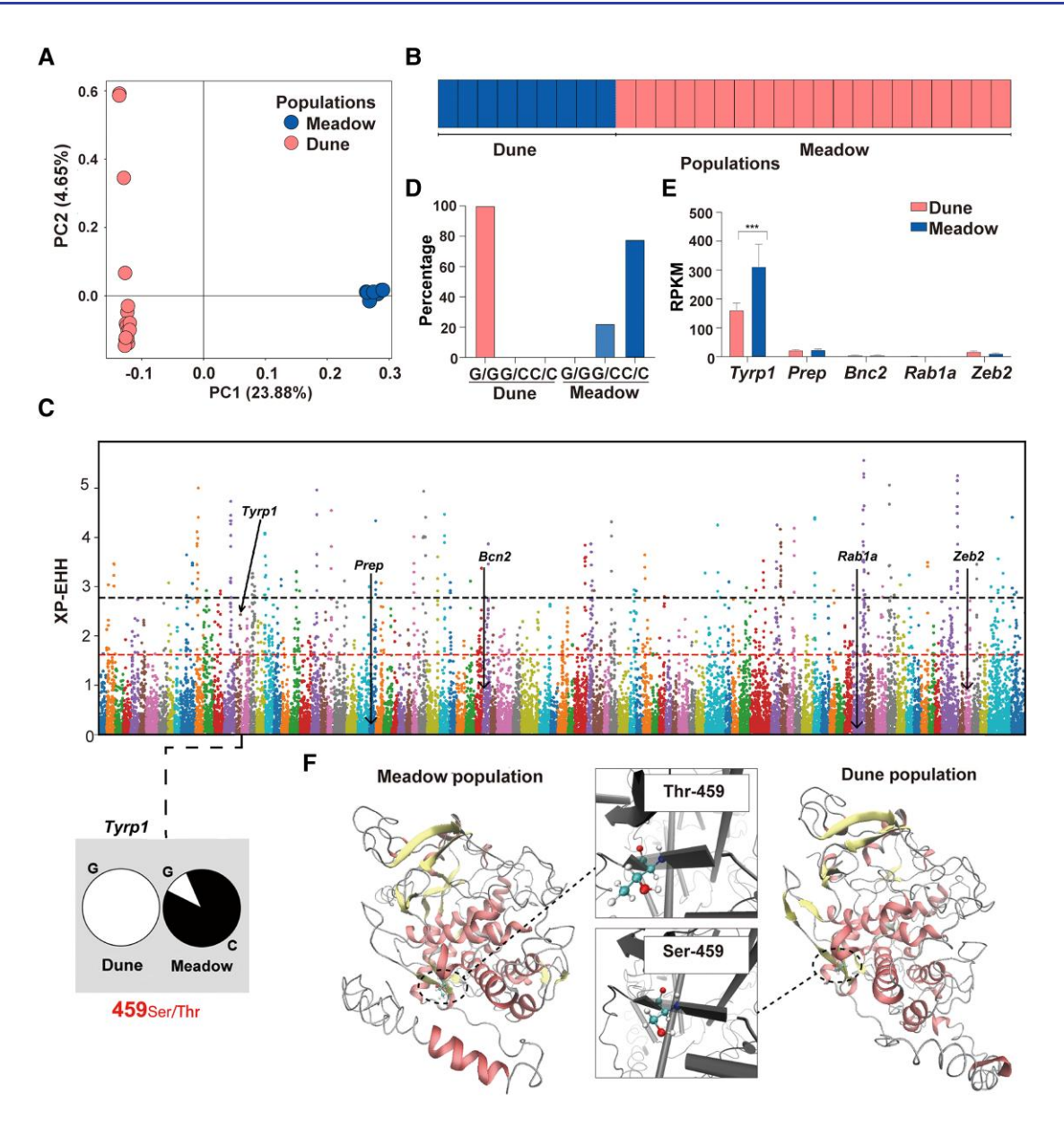


**Fig. 3.** Genomic and transcriptomic analysis of the phylogenetic relationship and mechanisms underpinning the dorsal coloration variations in lizards from the dune and alpine meadow populations. a) PCA analysis of the phylogenetic relationship between the dune and meadow populations. The first two axes of PCA for the dune (pink) and meadow (blue) populations are based on 7,146,131 SNPs. b) Individual assignment probability bar plot at the best fit (K = 2), inferred by Admixture and based on 642,957 neutral SNPs. c) The distribution of XP-EHH values that were calculated with a 40-kb window in a 20-kb step size between the dune and alpine meadow populations. The positions of the arrows represent the XP-EHH values of each candidate gene. The black and red dash lines indicate the top 1% and top 5% of XP-EHH, respectively. Notably, only Tyrp1 surpasses the threshold for the top 5% XP-EHH (i.e. 1.61879). d) The percentage of G/G, G/G, and G/G at G/G while lizards from the dune and alpine meadow populations by genomic resequencing. Lizards from the dune population have 100% G/G, while lizards from the meadow population possess G/G (22.22%) or G/G (77.78%) genotypes at G/G at G/G and G/G are G/G and G/G and G/G are G/G and G/G and G/G are G/G are G/G and G/G are G/G and G/G are G/G and G/G are G/G are G/G and G/G are G/G and G/G are G/G are G/G and G/G are G/G and G/G are G/G are G/G and G/G are G/G and G/G are G/G are G/G and G/G are G/G are G/G are G/G and G/G are G/G are G/G are G/G are G/G and G/G are G/G are G/G are G/G and G/G are G/G are G/G and G/G are G/G are G/G are G/G are G/G are G/G and G/G are G/G are G/G are G/G and G/G are G/G ar

Tyrp1 OE groups at 36 hpf (supplementary fig. S5e, Supplementary Material online) and 4 dpf (Fig. 4f), respectively. Additionally, surficial areas of ventral melanin significantly increased at 4 dpf (Fig. 4g). Interestingly, the Tyrp1<sup>1376C</sup> (dark) mRNA-injected group showed a significantly increased surficial area of dorsal melanin compared to the Tyrp1<sup>1376G</sup> (light) group (Fig. 4f). These findings suggest that the Tyrp1 from P. putiatai could efficiently promote zebrafish

melanin biosynthesis, and that the *Tyrp1*<sup>459Thr</sup> derived from the alpine meadow population may have higher melaningenerating potential compared to *Tryp1*<sup>459Ser</sup> derived from the dune population. Finally, we confirmed a significant upregulation of melanin in *Tyrp1* OE groups, and that the *Tyrp1*<sup>459Thr</sup> derived from the alpine meadow population led to more melanin biosynthesis activity than did the *Tyrp1*<sup>459Ser</sup> from the dune population (Fig. 4h).

**Table 1** The numbers of salt bridges, hydrogen bonds, radius of gyration, and solvent-accessible surface area of enzyme TYRP1 in the dorsal skin of lizards from alpine meadow (dark, Thr-459#) and dune populations (light, Ser-459#), respectively

	Salt bridges	Hydrogen bonds	Radius of gyration	Solvent-accessible surface area
Thr-459# (dark)	34	99	22.81	22,694
Ser-459# (light)	41	126	23.32	22,083

### **Discussion**

Here we found that the dark and light dorsal coloration in adjacent populations of *P. putjatai* facilitates both camouflage and thermoregulation in their respective habitats that differ in substrate color and thermal quality (e.g. dark and cold vs. light and warm). More interestingly, an important point mutation (different allele frequencies of G/C at the site of SNP 459# in the gene of *Tyrp1*) was found resulting in skin coloration variations that were positively selected for both camouflage and thermoregulation.

The divergence between alpine meadow and dune populations of P. putiatai happened at ~0.26 Ma, following the formation of Qinghai Lake and the appearance of dunes (2.43 to 0.73 Ma) (Hong et al. 2009). Our results of camouflage and thermoregulation experiments suggest that predators and thermal environments may additively shape the dorsal coloration variation between the alpine meadow and dune populations (Yang et al. 2020; Semenov et al. 2021). However, pinpointing the exact relative importance of these two ecological factors in driving dorsal coloration evolution over time is challenging, because the arrival time of avian ( $\sim$ 3.0 Ma) and mammalian (~1.7 Ma) predators of P. putjatai in the QTP predates the formation of dunes and, thus, the dune population of P. putjatai (He et al. 2021). Nonetheless, according to high attack rates by predators (Fig. 2c) and similar active body temperatures of lizards (Fig. 2d and e) we observed in this study, we infer that the selection pressure due to thermoregulation might not be as influential as the selection for camouflage. This inference is particularly supported by the higher attack rates if the lizard models were placed outside their matching habitats (Fig. 2c). Further investigations into the interplay of these factors could provide a more comprehensive understanding of the selective forces shaping dorsal coloration in P. putjatai (e.g. Rosenblum et al. 2010; Hardwick et al. 2015; Gunderson et al. 2022).

The functions of camouflage and thermoregulation may conflict in shaping animal coloration if one is compromising the other (e.g. Smith et al. 2016). In contrast, we demonstrated that the two functions turned out to be compatible, given that the dorsal coloration variation of lizards enhanced both camouflage and thermoregulation simultaneously in contrasting environments of dark and cold vs. light and warm. This compatibility is plausibly due to the fact that the selective pressures of camouflage and thermoregulation in shaping lizard coloration are consistent. The color matching between dorsal skins and habitat

substrate led to relatively low probabilities of predation attack in their respective natural habitats (Fig. 2b), indicating the role of crypsis as seen in other animals (Stevens and Merilaita 2009, 2011; Stuart-Fox and Moussalli 2009). Simultaneously, the lower dorsal reflectance and higher heating-up rates allow the dark lizards to effectively thermoregulate in the cold meadow environment to achieve higher body temperatures (Tao 2022). Consistent with the prediction of TMH, the dorsal coloration divergence is also likely an adaption to local thermal environments (Clusella-Trullas et al. 2007). Similarly, pale morphs of three lizard species (Eastern Fence Lizard [Sceloporus undulatus], Little Striped Whiptail [Aspidoscelis inornata], and Lesser Earless Lizard [Holbrookia maculata]) were found successfully colonized and adapted to the White Sands of New Mexico in North America (Rosenblum et al. 2004, 2007, 2010), by increasing camouflage against avian predators (Hardwick et al. 2015), and maintaining thermal performance as well (Gunderson et al. 2022).

We found that the Tyrp1 gene possessed a nonsynonymous mutation (Tyrp1459Thr/Ser) that is responsible for the between-population divergence in dorsal coloration in P. putjatia. This assertion is supported by several lines of evidence. First, the frequency of the mutation was stable in dark (Tyrp1459Thr) and light (Tyrp1459Ser) lizards from the alpine meadow and dune populations, respectively (Fig. 3c and d). Second, the mutation of Tyrp1 leads to fewer salt bridges and hydrogen bonds and thereby lower  $K_M$  value in the enzyme of TYRP1 from dark lizards, producing a more flexible structure of the enzyme TYRP1 with a higher catalytic ability (Pan et al. 2017; Kroll et al. 2021). The higher catalytic activity of TYRP1 may generate more eumelanin and total melanin content in alpine meadow lizards compared to their dune counterparts (supplementary fig. S3b and c, Supplementary Material online). Third, the mutation of Tyrp1 in the meadow population (Tyrp<sup>1376C</sup>) induced more melanin generation and resulted in a larger dark area on the skin surface than did Tyrp1 1376G from the dune population and in WT zebrafish (Fig. 4e to g). Notably, the darker dorsal coloration in alpine meadow lizards is attributable to the higher catalytic activity of TYRP1 due to genetic mutation, because the mutation of Tyrp1 did not affect the amount of enzyme TYRP1 or melanocytes (Fig. 4c; supplementary fig. S5b and d, Supplementary Material online). Analogous to our results, mutation and regulation in important genes (e.g. Mc1r, Prep, and Prkar1a) of the melanin-generating signal transduction pathway may lead to body coloration variation in lizards and other vertebrates as well (e.g. Braasch et al. 2009; Corso et al. 2012; Utzeri et al. 2014; Corl et al. 2018; McNamara et al. 2021). For example, the pale coloration of the lizards (S. undulatus, A. inornata, and H. maculata) has evolved background-matched coloration (i.e. blanched) at White Sands of New Mexico, through different mutations in Mc1r (Rosenblum et al. 2010). Similarly, the camouflage by pale coloration of beach mice from the dunes of Florida's coast is also achieved partly by a single amino acid mutation in Mc1r (Steiner et al. 2007).

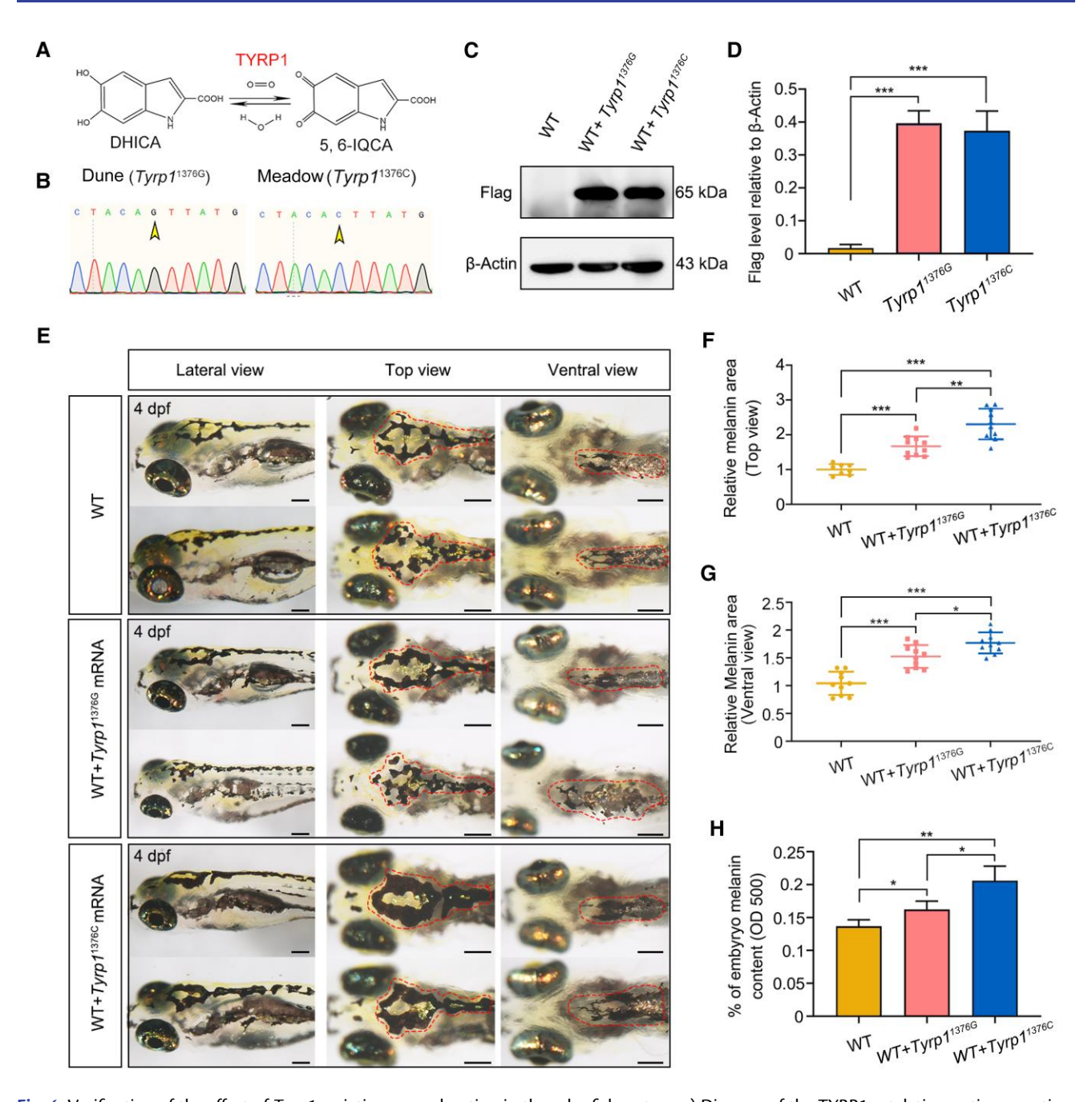


Fig. 4. Verification of the effect of Tyrp1 variations on coloration in the zebrafish system. a) Diagram of the TYRP1 catalytic reaction equation. b) The sequencing base peak of constructed  $Tyrp1^{1376G}$  (light color/dune population) and  $Tyrp1^{1376G}$  (dark color/alpine meadow population) OE vectors. The base changes are denoted by yellow arrowheads. c) Protein level of Flag-tagged TYRP1 in the WT,  $Tyrp1^{1376G}$  (light/dune), and  $Tyrp1^{1376G}$  (dark/meadow) mRNA OE groups detected by western blot. d) Quantification of protein level in (c) by using Gel-Pro analyzer. Data are shown as mean  $\pm$  so. \*\*\*P < 0.001. e) The representative bright-field images of zebrafish embryo melanin enriched area at 4 dpf in WT,  $Tyrp1^{1376G}$  and  $Tyrp1^{1376G}$  mRNA OE groups. The red dashed areas indicate regions with melanin enriched. From left to right panels are lateral, dorsal, and ventral views (scale bar, 200 µm). f) Quantification of relative melanin area of dorsal views in (e) by Image-Pro Plus analyses. Data are shown as mean  $\pm$  so. N (WT) = 8, N ( $Tyrp1^{1376G}$  OE embryo) = 10, N ( $Tyrp1^{1376G}$  OE embryo

Nonetheless, the detailed molecular regulatory mechanisms underlying the dorsal coloration variation in *P. putjatia* warrant further studies. For example, why the mutation of *Tyrp1* <sup>1376C</sup> enhances TYRP1 activity but not mRNA expression and its enrichment in the precursors of eumelanin remains unanswered.

Revealing the link between genotype, phenotype, and fitness can provide important insights into the process of local adaptation that starts with divergent/disruptive selection in different environments (Barrett and Hoekstra 2011; Rausher and Delph 2015). Here, we show that co-selection by camouflage and thermoregulation on the body coloration of

lizards resulted in a fixation of the allele in Tyrp1 in response to adjacent contrasting thermal environments and background colorations, despite the considerable gene flow between different ecotypes. This provides an excellent model system to further explore the mechanisms that promote adaptation and even speciation. In this study, the alleles retained in the dune population (i.e. 100% G/G) originate from standing genetic variation present in the meadow population (a mix of C/C, G/C, and G/G). This implies that the dune population can be considered as a derived population stemming from the meadow population. However, we need to exercise extreme caution in concluding that the dune population (i.e. derived) originated from the meadow population (i.e. ancestral) with such a limited number of populations in this study. For a more robust conclusion, it is essential to conduct a comprehensive analysis that includes additional populations, especially those beyond the current study area, and incorporates them into demographic inference models (e.g. Steiner et al. 2009). Therefore, some important questions for future studies include: (1) how does multifarious selection function during the process of local adaptation? (Chevin et al. 2014); (2) what is the role of gene flow during the fixation of mutation? (Pinho and Hey 2010); (3) how does ecological adaptation interact with phylogenetic evolution in determining the current pattern of body coloration? Such work requires joint endeavors from both ecologists and molecular biologists to identify the ecological processes and evolutionary mechanisms involved.

#### **Materials and Methods**

#### Study System

The toad-headed agama (*P. putjatai*) is a small viviparous lizard (snout-vent length [SVL] < 70 mm) on the QTP (Hu et al. 2019). This species is distributed in the Gobi or semidesert dune areas of the Qinghai Lake Basin, and the alpine meadows around Qinghai Lake, with elevations ranging from 2,500 to 3,500 m asl (https://www.iucnredlist.org/species/47755672/47755678) (Jin et al. 2014). Populations of *P. putjatai* not only experience dramatic climate fluctuation but also face predation pressure exerted by birds and mammals (Li 1989). *P. putjatai* expresses distinct body coloration among populations, with dark dorsal coloration in lizards inhabiting the alpine meadow where the substrate is dark loam, and light dorsal coloration in lizards inhabiting dunes by Qinghai Lake where the substrate is light sand.

In July 2019, we collected 38 dark lizards from an alpine meadow population (100.999°E, 37.083°N; elevation 3,280 m asl), and 35 light lizards from a dune population by Qinghai Lake (100.866°E, 36.682°N; elevation 3,330 m asl) (supplementary fig. S6a, Supplementary Material online). We took photos of lizards in natural habitats (supplementary fig. S6b, Supplementary Material online) with a spectrum camera (Specim IQ, Specim Ltd., Oulu, Finland) before they were transferred to our laboratory in Beijing. We used a 2 (population) × 2 (substrate) design

to detect the plasticity of dorsal coloration. Both the dark and light lizards were reared in two treatments with meadow and dune substrates collected from our field study sites, respectively. We reared four lizards in each terrarium  $(550 \times 420 \times 360 \text{ mm})$  with 50 mm depth of substrates, which were located in oxygen-controlled chambers (14.5% oxygen concentration,  $600 \times 550 \times 960$  mm) in a temperature-controlled room at  $16 \pm 1$  °C. A heating lamp (25 W) was hung above one end of each terrarium to create a thermal gradient of 16 to 40 °C for lizard thermoregulation from 8 AM to 8 PM. Food (crickets dusted with vitamin supplements) and water were provided ad libitum. After 2 mo, we took photos of lizards again to detect the plasticity of the dorsal coloration of lizards (supplementary fig. S6c, Supplementary Material online). In addition, we collected pregnant females from the alpine meadow (black, n = 6) and dune (light, n = 6) populations, and reared them in the indoor laboratory in the same way as described above  $(2 \times 2 \text{ design})$ . We took photos of the neonates produced by the females to identify the between-population variation under different substrates in dorsal coloration in offspring (supplementary fig. S6d, Supplementary Material online). Our preliminary results indicated that the difference in dorsal coloration of lizards from the alpine meadow and dune populations was not induced by developmental plasticity (see detail results in supplementary fig. S6, Supplementary Material online), because the neonates of the two populations showed distinct dark and light dorsal colorations as seen in adults, and the between-population difference in dorsal coloration was still significant after the lizards from the two populations were kept on the same substrate in the laboratory for 2 mo. Therefore, the contrast in microhabitats and dorsal coloration of P. putjatai in adjacent populations provides an excellent model system for investigating the functions and underlying genetic mechanisms of body coloration, with particular attention to ecological adaptation.

From early June to early July 2020, we collected adult P. putjatai from three alpine meadow populations with dark dorsal coloration (36.97° to 37.09°N, 100.88° to 100.99°E; elevation 3,212  $\pm$  35 m asl) and three dune populations with light dorsal coloration (36.64° to 37.06°N, 100.53° to 100.88°E; elevation  $3,257 \pm 18 \text{ m}$  asl) beside Qinghai Lake on QTP, respectively. First, we verified the taxonomic status of the six populations of P. putjatai. We selected two lizards from each of the six populations to extract total genomic DNA from blood. We amplified one mitochondrial DNA (mtDNA) gene fragment, 1,096 bp of ND2, and exons of one nuclear DNA (nuDNA) gene, 634 bp of BDNF. The total length of these data was 1,730 bp. Primer pairs for PCR were taken from the literature (BDNF: Townsend et al. 2008; ND2: Noble et al. 2010). PCR products were sequenced with both forward and reverse primers using Applied Biosystems 3,730 DNA Analyzer (Applied Biosystems, Carlsbad, CA, USA). We obtained the sequences for Phrynocephalus myctaceus and P. vlangalii from published data as outgroups, as well as one sample of P. putjatai from Guide County, where is outside our study area (Solovyeva et al. 2018). Sequences were first aligned using the Clustal Omega (Sievers et al. 2011), in Geneious Prime 2022.1.1 (http://www.geneious.com/) with default parameters. Subsequently, the alignment was checked and manually revised if necessary. Phylogenetic analyses were performed with a concatenation of all genes. We reconstructed the phylogenetic tree under the maximum likelihood (ML) by using RaxML 8.2.11 with 100 bootstrap replicates (Stamatakis 2014), employing the standard GTR + GAMMA model of nucleotide substitution. Then, using one pair of populations that have typical dark and light colorations (i.e. dark 1 and light 3 in Fig. 1; dark: 37.09°N, 100.99°E, 3,259 m asl; light: 36.64°N, 100.88°E, 3,280 m asl), we compared the functions and underlying mechanisms of dorsal colorations between two ecotypes of lizards.

## Reflectance Spectra of Microhabitat and Dorsal Skin of Lizards in the Field

The camouflage function of dorsal coloration occurs mostly within the range of the visible spectrum e.g. birds: 300 to 700 nm, and mammals: 400 to 700 nm (e.g. Ma et al. 2019; Stoddard et al. 2020). Thus, we first determined the reflectance spectra of microhabitat substrates and dorsal skin of lizards using a miniaturized handheld hyperspectral camera (400 to 1,000 nm; Specim IQ, Specim Ltd., Oulu, Finland). On sunny days, we took photos of dark and light lizards in their natural habitats, and determined the reflectance spectra of substrates and lizards synchronously (supplementary fig. S6b, Supplementary Material online). For the analysis, we first extracted eight to ten spots randomly on the surface of the substrate and dorsal skin of the lizard, respectively. Subsequently, we obtained the reflectance curve for each spot by the software ENVI 5.3 (Harris Geospatial Solutions, Inc., USA), and recorded the average reflectance of each curve across the wavelength from 400 to 1000 nm for each spot. Then we averaged the reflectance value of the eight to ten spots as the reflectance value for each substrate and lizard, respectively. The reflectance value was expressed as %, indicating the percentage of the spectrum which were reflected by the surface of the substrate or dorsal skin of the lizard. The differences in average reflectance spectra between the lizard and the substrate were then calculated. We employed SPSS V21.0 to analyze the data. We used generalized linear models to detect the difference between the average reflectance spectra of substrate and lizards from dunes and alpine meadow habitats respectively, with population as the main factor.

#### The Role of Dorsal Coloration in Camouflage

After reflectance spectra determination, we determined the camouflage functions of the dorsal coloration, using plasticine models that mimicked lizards with different colors. We made a silastic mold of the lizard with the specimen of an adult *P. putjatai*, and then filled fresh, nontoxic (i.e. foodgrade) and flavorless plasticine into the mold to shape the

lizard models. After several minutes of drying, the lizard models made in plasticine were ready. The colorations of the models were regulated by the mixture of white and yellow plasticines for the models mimicking the lizards of the dune population, and by the mixture of white and black plasticines for the models mimicking the lizards of the meadow population (supplementary fig. \$7a and b. Supplementary Material online). The dorsal patches of lizard models were painted with nontoxic (i.e. food-grade) and flavorless pigment (supplementary fig. S7c and d, Supplementary Material online). The proportions of the mixed plasticines and the mixed pigment were according to the formula determined in the preliminary experiment. The brightness of models and lizards was analyzed by oneway ANOVAs, the similar brightness between the plasticine models and lizards indicated that the models were valid in mimicking the dorsal colors of light and dark lizards (supplementary fig. S2e, Supplementary Material online).

The plasticine lizard models were then used for camouflage determination. In brief, we placed 44 light and 44 dark lizard models in the dune habitat, and 45 light and 47 dark lizard models in the alpine meadow habitat. On sunny days plasticine lizard models were placed in pairs at intervals of 2 m along two parallel transects in the alpine meadow and dune habitats, respectively. Models were set out at 10 AM to 11 AM on the first day and retrieved at the same time on the second day. We then counted the number of lizard models that showed traces of being attacked by predators to evaluate the role of dorsal coloration in camouflage (supplementary fig. S7f to i, Supplementary Material online). The traces of being gnawed or pecked were considered as being attacked as the predators of P. putjatai mainly are avians and mammals. We repeated the experiment twice at the meadow and dunes, respectively, and the results were repeatable. The ratio of models that were attacked vs. not attacked was analyzed using Chi-square tests, to compare differences in predation attempts between light and dark lizard models in the dune and alpine meadow habitats.

#### The Role of Dorsal Coloration in Thermoregulation

To quantify operative temperatures ( $T_{\rm e}$ ), we placed copper models of a similar size to the lizards (length × width × height,  $70 \times 25 \times 10$  mm) in their natural habitats from late June to mid-August 2020. We set out six models for each population, including two models at open, filtered, and shaded sites, respectively. We placed one temperature logger (iButton, DS1921; Maxim Integrated Products Ltd.) in each copper tube model to record hourly temperatures (Liu et al. 2022). From each set of six temperature loggers, we calculated the average  $T_{\rm e}$  for each population.

In addition, during the daily active period of lizards from 9 AM to 5 PM on sunny days, we captured lizards by lasso or hand, and immediately measured body temperature ( $T_b$ , cloacal temperature). Additionally, we measured the substrate surface temperature ( $T_{surface}$ ), and air temperature (30 cm height from the surface) ( $T_{air}$ ) with electronic thermocouples (UNT-325, Shanghai, China) at the same

sites from which lizards were captured. We collected 122 and  $270T_b$  for lizards in the meadows and dunes, respectively. We used a dependent t-test to compare the differences in operative temperatures ( $T_e$ ) between the dune and alpine meadow microhabitats. Next, we used generalized linear models to analyze the differences in substrate surface temperature ( $T_{\rm surface}$ ), air temperature ( $T_{\rm air}$ ), and active body temperatures ( $T_b$ ) between dune and alpine meadow habitats, with the origin of the population as the main factor, and time as a covariate.

After measurements of active body temperatures, we transferred 40 lizards from each population for further experiments. To compare the heating-up rate between dark and light lizards, we conducted a heating-up experiment with a full-spectrum heating lamp (220 V, 50 W; Hanyang, China) to calculate the thermal time constant  $(\tau)$  of lizards in the laboratory (Dzialowski and O'Connor 2001). As heating functions of radiation are mostly within a wide wavelength (e.g. 300 to 700 nm provides 45% heat, 700 to 2,500 nm provides 50% heat) (Stuart-Fox et al. 2017), we additionally determined the dorsal skin reflectance in the laboratory under a full spectrum lamp (400 to 1,700 nm) using the Specim system (Specim FX, Specim Ltd., Oulu, Finland). The results of the reflectance were similar to previous records. Lizards were acclimated at 15 °C for 2 h and then attached to an insulated panel (Expanded Polystyrene, EPS, 400 × 300 mm) with doublesided tape. A heat lamp was suspended 60 cm above the lizards. We recorded the dorsal body temperatures of lizards from 15 °C every 10 s with a calibrated electric thermometer (835-T1, Testo, Germany). We calculated the thermal time constant ( $\tau$ ) at 30 °C (time to increase body temperatures from 15 to 30 °C), and body temperature increase within 5 min from 15 °C to evaluate the heating-up rates of lizards (Dzialowski and O'Connor 2001). We used general linear models to analyze the average reflectance spectra with the origin of the population as the main factor. We also used general linear models to analyze the thermal constant time  $(\tau)$ , and the increase of the body temperatures in 5 min intervals, with the origin of population as the main factor, and initial body temperature, SVL, and body mass as covariates.

#### Melanin Abundance in Dorsal Skin

We evaluated the melanin abundance in dorsal skin using two estimates: the surficial area of melanin and the content of eumelanin and total melanin (i.e. the total content of eumelanin and phaeomelanin combined). First, we performed optical microscopy to analyze the surficial area of total melanin on the dorsal skin of the lizards from the dune and alpine meadow populations. Lizards were acclimated at 15 °C for 2 h (which is the body temperature at which lizards become active in the field). Then we sacrificed the lizards by euthanasia and immediately collected samples of dorsal skin at 15 °C. Dorsal skin samples were collected from the same area in which the reflectance spectrum of dorsal coloration had been measured previously. Dorsal skin samples were immersed in 4% paraformaldehyde for 2 d at 4 °C and

then washed in water for over 30 min. We dehydrated the dorsal skins in a graded series of alcohol, penetrated with a xylene–alcohol mixture (1:1), then xylene. Finally, we took images of dorsal skins using a Nikon NIS elements F imaging system (4.60.00, Nikon, Tokyo), which was linked to an optical microscope set as 10 objective lenses × 10 ocular lenses. The surficial area of total melanin was then calculated by the software Image-Pro Plus 6.0.0.260 (ImagePro, Dallas, TX). In brief, for each microscope view, the total area was equivalent to 1,779,968 ppi. Pixels of total melanin were labeled with red color. We then calculated the numbers of ppi in the red area out of 1,779,968 per view (supplementary fig. S8, Supplementary Material online).

Second, we measured the content of eumelanin and total melanin of dorsal skins using a spectrophotometer, according to published protocols with minor modifications (Ozeki et al. 1996). First, we obtained a standard curve with melanin, and then tested the content of eumelanin and total melanin according to absorbance. For each test, we used 20 mg dorsal skin cut into pieces and placed in 100 µL cell lysis solution (Solarbio Life Science, Beijing, China). The skin pieces were acclimated at 4 °C for 30 min and then centrifugated at  $12,000 \times g$  for 10 min. The sediment was then added to 1 mL NaOH solution (3 mol/L) and acclimated at 80 °C for 2 h. The skin sample suspension was then tested at 500 nm (A500) and 650 nm (A650) with a spectrophotometer. Total melanin content was calculated by a standard curve equation with the values from A500 (melanin concentration =  $0.447 \times A500 - 0.018$ , mg/g). The ratio of A650/A500 was then calculated to estimate the content of eumelanin (Ozeki et al. 1996).

We also conducted metabolite analysis with dorsal skins from the dune and alpine meadow populations. The metabolites involved in the melanin-generating pathway were analyzed by Biomarker Technologies Corporation following the established protocols (Zhu et al. 2019). In brief, 15 samples of dorsal skins (100 mg per sample) from each population were used for analysis. We obtained the data by extraction, sample testing, liquid chromatographymass spectrometry (HLPC-MS), metabolite quantification, and identification. The raw data were then assessed using Progenesis QI software (Nonlinear Dynamics, USA). We normalized the relative abundance of each peak and then generated a peak graph and detected the metabolite database. Next, we searched for the metabolites related to melanin generation and recorded the relative abundance for each sample. Surface areas, eumelanin content, and total melanin content in dorsal skin were analyzed using a generalized linear model, with the origin of the population as the main factor. Between-population differences metabolites in the melanin-generating pathway of dorsal skins were analyzed by Mann-Whitney U tests.

# Whole-genome Resequencing and Transcriptomic Sequencing

We conducted whole-genome resequencing and transcriptomic sequencing to reveal the molecular regulation

of coloration in lizards from alpine meadow and dune populations. For genomic resequencing, we collected muscle samples from lizards after euthanasia (N = 9 for the alpine meadow population and N = 20 for the dune population) and immediately transferred the tissues into liquid nitrogen. The libraries were sequenced to an approximate depth of 10x on the Illumina NovaSeq 6000 platform, employing paired-end reads with a length of 150 bp (Novogene Corporation, Beijing, China). We used BWA (Burrows-Wheeler Aligner) (Version: 0.7.8) (Li and Durbin 2009) with "mem -t 4 -k 32 -M" to map the raw reads of each individual to the P. vlangalii genome (https://bigd.big.ac.cn/search/?dbId=gwh&q= GWHAAFC00000000) (Gao et al. 2019) (supplementary tables S5 and S6, Supplementary Material online). The variant calling was performed according to all the aligned BAM files using "mpileup" in SAMtools (Li et al. 2009) with the parameters "-q 1 -C 50 -t SP -t DP -m 2 -F 0.002'. To obtain high-quality SNPs for downstream analysis, we retained SNPs with the following criteria: coverage depth  $\geq$ 5 and  $\leq$ 100, RMS mapping quality  $\geq$  20, maf > 0.1, and missing rate < 0.1 (supplementary table S7, Supplementary Material online).

We scanned for signals of selection across the genome using XP-EHH scores (Sabeti et al. 2007) as implemented in the Python package "ALLEL" (DOI: 10.5281/zenodo.4759368) with a sliding window of 40 Kb in 20 Kb step size. Genomic regions with extreme XP-EHH scores (top 5%) were considered as candidate regions under rigorously selective sweeps. All outlier regions were assigned to corresponding SNPs and annotated genes. We then took the SNPs in windows with FDR > 0.05 as neutral. which were used to reveal the population structure and infer the demographic history of the dune and alpine meadow populations. The calculation of pairwise  $F_{ST}$  and PCA was based on all the SNPs that passed the quality control by SAMtools (7,146,131 SNPs). Pairwise  $F_{ST}$  (Weir and Cockerham 1984) between the dune and alpine meadow populations was obtained with VCFtools (Danecek et al. 2011), and PCA was carried out with EIGENSOFT (Patterson et al. 2006). We then evaluated population structure using genetic clustering analysis ADMIXTURE (Alexander et al. 2009), which was based on all the neutral SNPs (642,957 SNPs). From K = 1 to 5, 100 independent runs were performed for each K with the default termination criteria per run. We used a 5-fold cross-validation procedure to choose the optimum K. For historical demographic analysis, four basic models were performed: a simple isolation model with no migrants (IS), a model with constant migration rate (IM), a model with ancient migration only (AM), and a model with secondary contact (SC). We used a FASTSIMCOAL 26 (Excoffier and Foll 2011) to perform the model selection based on the site frequency spectrum (SFS) of the neutral SNPs. The input was transformed from vcf files by vcf2sfs.py of Popgen Pipeline Platform (PPP, https:// github.com/jaredgk/PPP.git). We used the mutation rate  $\mu = 2e-9$  from Gao et al. (2022). All models were

compared using the Akaike Information Criterion (AIC) from the approximated likelihood and number of parameters. One hundred replicates were run for each model to obtain the highest likelihood. Each run included 100,000 simulations for estimating the composite likelihood and 50 cycles by each time using a conditional maximization for estimating parameters.

For transcriptomic sequencing, we collected skin tissue samples of six captive individuals from each population (12 lizards in total) immediately after euthanasia in the indoor laboratory, and transferred the skin tissue into liquid nitrogen. We prepared one paired-end library for each individual. Libraries were sequenced using the Illumina Novaseq platform (Performed by Novogene Corporation) with a read length of 150 bp, which produced ~6 Gb high-quality reads for each sample. The mapping of RNA-seq clean reads to the indexed reference genome was conducted with HISAT2 v2.0.4 program with default parameters (Pertea et al. 2016) (supplementary table S8, Supplementary Material online). Fragments per kilobase of transcript per million mapped reads (FPKM) is one of the most commonly used methods for estimating gene expression levels, which considers the effect of sequencing depth and gene length for the reads count at the same time. We counted the mapping rates of reads to each gene with HTSeq v0.6.1 (Anders et al. 2015) and calculated FPKM for each gene. Differential-expression analysis was performed by the EdgeR (Robinson et al. 2010).

To further examine the differences in Tyrp1 between the alpine meadow and dune populations in sequence, we amplified the Tyrp1 gene for 30 individuals from each of the meadow and dune populations, respectively, by PCRs in 2022. We designed a pair of primers for the Tyrp1 sequence with PRIMER 3.0 online (Andreas et al. 2012). (TYRP1-F: AGCTCAATATACCCAATAGAA; TYRP1-R: TGAGCGAACGAACGAAT). PCRs were performed in a 25 µL reaction volume containing 12.5 µL Premix Ex Taq II Version 2.0 (2x; Takara Biotechnology [Dalian] Co., Ltd), 0.1 µM of each PCR primer and 80 ng of genomic DNA. The PCR products were sequenced directly in the forward direction on an ABI 3730 capillary sequencer (Applied Biosystems, Life Technologies, New York, USA) using a BigDye Terminator v3.1 Cycle Sequencing Kit (Life Technologies, New York, USA).

## Model-predicted Structure and Catalytic Activity of TYRP1 Between the Dune and Alpine Meadow Populations

Corresponding to the sequence differences between the dune and alpine meadow populations (see details in results of Genomic resequencing), we projected the 3-D structures of the most important candidate enzymes (i.e. TYRP1) in melanin generation, the genetic sequence of which differed between dune and alpine meadow populations. We then performed integrative modeling with Iterative Threading ASSEmbly Refinement (I-TASSER) (Zhang 2008), by using the software Visual Molecular

Dynamics (VMD) to visualize the structure of the enzyme of TYRP1 (Humphrey et al. 1996). C-scores of 3-D structures are calculated based on the significance of threading template alignments and the convergence parameters of the structure assembly simulations for estimating the quality of predicted models. C-score is typically in the range between -5 and 2, and a higher value signifies a model with high confidence (Zhang 2008). We then calculated the numbers of the salt bridges, hydrogen bonds, radius of gyration, and solvent-accessible surface area of the structure in the dune and alpine meadow populations, respectively.

Further, we predicted the catalytic activity (i.e.  $K_{\rm M}$  value) of TYRP1 in the dune and alpine meadow populations according to sequence and structure, following the model developed by Kroll et al. (2021). This model can predict enzyme activity based on its structure. In brief, this is a deep-learned model based on the UniRep vectors of enzymes and the diverse molecular fingerprints of their substrates. We modified it to achieve the prediction of  $K_{\rm M}$  value with amino acid sequences and the structure of individual enzymes and the ID in KEGG of the corresponding substrates as input. To compare  $K_{\rm M}$  values, we input the sequence of the enzyme TYRP1 from the dune and alpine meadow populations, respectively.

## Functional Verification of *Tyrp1* in Melanin Generation

To verify the functional differences in the mutation of Tyrp1 from the dune and alpine meadow populations in melanin generation, we performed functional verification using a model Zebrafish system. The Zebrafish line Tübingen (WT) was raised in system water at  $28 \pm 0.5$  °C under standard conditions. Zebrafish embryos were obtained by natural spawning and raised in an incubator at 28 °C. In brief, we verified the functions of Tyrp1 by mRNA microinjection. For P. putjatai, Tyrp1 mRNA overexpression, Flag-tagged Tyrp1<sup>1376G</sup> (i.e. light) and Tyrp1<sup>1376C</sup> (i.e. dark) CDs were cloned into pCS2+ vectors. The mRNAs were then generated by using SP6 mMessage Machine kit (AM1340; Ambion) and 100 to 200 pg of mRNAs were injected into embryos at the one-cell stage. To confirm the expression of TYRP1 after mRNA injection, western blotting was performed at 36 hpf as previously reported (Lv et al. 2020) using the following antibodies: anti-β-Actin antibody (4967; Cell Signaling Technology), and anti-Flag antibody (F7425; Sigma-Aldrich). Relative protein level was calculated by 8-bit gray analysis (Gel-Pro analyzer 6.3). We also performed microscopy imaging for comparison of the darkness of zebrafish between Tyrp1 1376G (light) and Tyrp1 1376C (dark) mRNA injections at 36 hpf or 4 dpf. The brightfield photographs of zebrafish were taken by using a Nikon SMZ1500 stereomicroscope and the raw images were processed by Image-Pro Plus, photoshop CC 2021. We used Student's t-tests to compare the differences in relative expression, melanin area, and melanin content between the groups of WT, Tyrp1 1376G (light), and Tyrp1 1376C (dark) mRNA injections.

## Supplementary Material

Supplementary material is available at Molecular Biology and Evolution online.

## **Acknowledgments**

We thank Yingjun Wang, Luyuan Ge, Zixuan Chen, and Wenjia Chen for their help with the field and laboratory work. We also thank Alexander Kroll for his help with the deep learning model. Many thanks to Tobias Uller, Nathalie Feiner, Xiao Xu, and Yuanting Jin for their comments on the manuscript.

#### **Author Contributions**

B.J.S., W.G.D., and F.L. conceived the ideas; B.J.S., C.Q.Y., Y.W., P.L., M.L.L., and G.N.W. designed methodology; B.J.S., W.M.L., P.L., D.Y.W., S.A.T., Z.W.J., H.X.X., and X.F.W. collected the data; B.J.S., W.M.L., P.L., G.N.W., and Y.W. analyzed the data; B.J.S. and W.G.D. led the writing of the manuscript. B.J.S., G.N.W., and W.G.D led the revising of the manuscript. All authors contributed critically to the drafts and gave final approval for publication.

## **Funding**

This work is supported by grants from The Second Tibetan Plateau Scientific Expedition and Research Program (STEP) (2019QZKK0501), The Strategic Priority Research Program of the Chinese Academy of Sciences (XDB31000000), Joint Grant from Chinese Academy of Sciences-People's Government of Qinghai Province on Sanjiangyuan National Park (LHZX-2020-01), National Key Research and Development Program of China (2022YFF0802300), and National Natural Science Foundation of China (32271572 and 32200341). B.J.S. is supported by Youth Innovation Promotion Association, Chinese Academy of Sciences.

Conflict of interest statement. The authors declare no conflict of interest.

## **Data Availability**

The experimental data, genome resequencing data, transcriptomic data, the amino acid sequences of *Tyrp1*, and the *Tyrp1* gene sequences for 30 lizards from the meadow population and 30 lizards from the dune population are available from the Science Data Bank (https://doi.org/10.57760/sciencedb.11683.). The input files used for FASTSIMCOAL2.6, output files, and observed site frequency spectra are available from the Figshare (https://doi.org/10.6084/m9.figshare.23675388.).

#### References

Alexander DH, Novembre J, Lange K. Fast model-based estimation of ancestry in unrelated individuals. *Genome Res.* 2009:**19**(9): 1655–1664. https://doi.org/10.1101/gr.094052.109.

- Anders S, Pyl PT, Huber W. HTSeq—a python framework to work with high-throughput sequencing data. *Bioinformatics*. 2015:**31**(2): 166–169. https://doi.org/10.1093/bioinformatics/btu638.
- Andreas U, Ioana C, Triinu K, Jian Y, Faircloth BC, Maido R, Rozen SG. Primer 3—new capabilities and interfaces. *Nucleic Acids Res.* 2012:**15**:e115. https://doi.org/10.1093/nar/gks596
- Aspengren S, Sköld HN, Wallin M. Different strategies for color change. Cell Mol Life Sci. 2009:66(2):187–191. https://doi.org/10.1007/s00018-008-8541-0.
- Barrett RD, Hoekstra HE. Molecular spandrels: tests of adaptation at the genetic level. *Nat Rev Genet*. 2011:**12**(11):767–780. https://doi.org/10.1038/nrg3015.
- Braasch I, Liedtke D, Volff J-N, Schartl M. Pigmentary function and evolution of tyrp1 gene duplicates in fish. *Pigment Cell Melanoma Res.* 2009:**22**(6):839–850. https://doi.org/10.1111/j. 1755-148X.2009.00614.x.
- Chevin LM, Decorzent G, Lenormand T. Niche dimensionality and the genetics of ecological speciation. *Evolution*. 2014:**68**(5): 1244–1256. https://doi.org/10.1111/evo.12346.
- Clusella-Trullas S, Terblanche JS, Blackburn TM, Chown SL. Testing the thermal melanism hypothesis: a macrophysiological approach. *Funct Ecol.* 2008:**22**(2):232–238. https://doi.org/10.1111/j.1365-2435.2007.01377.x.
- Clusella-Trullas S, van Wyk JH, Spotila JR. Thermal melanism in ectotherms. J Therm Biol. 2007;32(5):235–245. https://doi.org/10.1016/j.jtherbio.2007.01.013.
- Corl A, Bi K, Luke C, Challa AS, Stern AJ, Sinervo B, Nielsen R. The genetic basis of adaptation following plastic changes in coloration in a novel environment. *Curr Biol.* 2018:**28**(18): 2970–2977.e7. https://doi.org/10.1016/j.cub.2018.06.075.
- Corso J, Gonçalves GL, de Freitas TRO. Sequence variation in the melanocortin-1 receptor (MC1R) pigmentation gene and its role in the cryptic coloration of two south American sand lizards. *Genet Mol Biol.* 2012:**35**(1):81–87. https://doi.org/10.1590/S1415-47572012005000015.
- Danecek P, Auton A, Abecasis G, Albers CA, Banks E, DePristo MA, Handsaker RE, Lunter G, Marth GT, Sherry ST, et al. The variant call format and VCFtools. *Bioinformatics*. 2011:**27**(15): 2156–2158. https://doi.org/10.1093/bioinformatics/btr330.
- Dzialowski EM, O'Connor MP. Thermal time constant estimation in warming and cooling ectotherms. *J Therm Biol.* 2001:**26**(3): 231–245. https://doi.org/10.1016/S0306-4565(00)00050-4.
- Excoffier L, Foll M. Fastsimcoal: a continuous-time coalescent simulator of genomic diversity under arbitrarily complex evolutionary scenarios. *Bioinformatics*. 2011:**27**(9):1332–1334. https://doi.org/10.1093/bioinformatics/btr124.
- Gao W, Sun YB, Zhou WW, Xiong ZJ, Chen L, Li H, Fu TT, Xu K, Xu W, Ma L, et al. Genomic and transcriptomic investigations of the evolutionary transition from oviparity to viviparity. Proc Natl Acad Sci U S A. 2019:**116**(9):3646–3655. https://doi.org/10.1073/pnas.1816086116.
- Gao W, Yu CX, Zhou WW, Zhang BL, Chambers EA, Dahn HA, Jin JQ, Murphy RW, Zhang YP, Che J. Species persistence with hybridization in toad-headed lizards driven by divergent selection and low recombination. *Mol Biol Evol*. 2022:**39**(4):msac064. https://doi.org/10.1093/molbev/msac064.
- Gunderson AR, Riddell EA, Sears MW, Rosenblum EB. Thermal costs and benefits of replicated color evolution in the White Sands desert lizard community. *Am Nat.* 2022:**199**(5):666–678. https://doi.org/10.1086/719027.
- Hardwick KM, Harmon LJ, Hardwick SD, Rosenblum EB. When field experiments yield unexpected results: lessons learned from measuring selection in White Sands lizards. PLoS One. 2015:10(2):1–18. https://doi.org/10.1371/journal.pone. 0118560.
- He J, Lin S, Ding C, Yu J, Jiang H. Geological and climatic histories likely shaped the origins of terrestrial vertebrates endemic to the Tibetan plateau. *Glob Ecol Biogeogr*. 2021:**30**(5):1116–1128. https://doi.org/10.1111/geb.13286.

- Heidrich L, Friess N, Fiedler K, Brändle M, Hausmann A, Brandl R, Zeuss D. The dark side of Lepidoptera: colour lightness of geometrid moths decreases with increasing latitude. *Glob Ecol Biogeogr.* 2018:**27**(4):407–416. https://doi.org/10.1111/geb.12703.
- Hendry AP, Huber SK, De León LF, Herrel A, Podos J. Disruptive selection in a bimodal population of Darwin's finches. *Proc R Soc B Biol Sci.* 2009:**276**(1657):753–759. https://doi.org/10.1098/rspb.2008.1321.
- Hong C, Zhangdong JIN, Zhisheng AN. Sedimentary evidences of the uplift of the Qinghai Nanshan (the mountains south to Qinhai lake) and its implication for structural evolution of the lake Qinghai-Gonghe basin. *Geol Rev.* 2009:**55**:49–57. https://doi.org/10.3321/j.issn:0371-5736.2009.01.006.
- Hu CC, Wu YQ, Ma L, Chen YJ, Ji X. Genetic and morphological divergence among three closely related *Phrynocephalus* species (Agamidae). *BMC Evol Biol.* 2019:**19**(1):114. https://doi.org/10.1186/s12862-019-1443-y.
- Humphrey W, Dalke A, Schulten K. VMD: visual molecular dynamics. J Mol Graph. 1996:14(1):33–38. 27-38. https://doi.org/10.1016/0263-7855(96)00018-5.
- Ito S, Wakamatsu K. Chemistry of mixed melanogenesis—pivotal roles of dopaquinone. *Photochem Photobiol*. 2008:**84**(3): 582–592. https://doi.org/10.1111/j.1751-1097.2007.00238.x.
- Jin Y, Brown RP. Morphological species and discordant mtDNA: a genomic analysis of *Phrynocephalus* lizard lineages on the Qinghai-Tibetan plateau. *Mol Phylogenet Evol.* 2019:**139**:106523. https://doi.org/10.1016/j.ympev.2019.106523.
- Jin Y, Yang Z, Brown RP, Liao P, Liu N. Intraspecific lineages of the lizard *Phrynocephalus putjatia* from the Qinghai-Tibetan plateau: impact of physical events on divergence and discordance between morphology and molecular markers. *Mol Phylogenet Evol.* 2014:**71**:288–297. https://doi.org/10.1016/j.ympev.2013.11.004.
- Kaelin CB, Barsh GS. Genetics of pigmentation in dogs and cats. Annu Rev Anim Biosci. 2013:1(1):125–156. https://doi.org/10. 1146/annurev-animal-031412-103659.
- Kroll A, Engqvist MKM, Heckmann D, Lercher MJ. Deep learning allows genome-scale prediction of Michaelis constants from structural features. *PLoS Biol.* 2021:**19**(10):e3001402. https://doi.org/10.1371/journal.pbio.3001402.
- Li D. Economic fauna of Qinghai. Qinghai: Qinghai People's Press; 1989.
- Li H, Durbin R. Fast and accurate short read alignment with Burrows-Wheeler transform. *Bioinformatics*. 2009:**25**(14): 1754–1760. https://doi.org/10.1093/bioinformatics/btp324.
- Li H, Handsaker B, Wysoker A, Fennell T, Ruan J, Homer N, Marth G, Abecasis G, Durbin R, Genome Project Data Processing Subgroup. The sequence alignment/map format and samtools. *Bioinformatics*. 2009:**25**(16):2078–2079. https://doi.org/10.1093/bioinformatics/btp352.
- Liu WL, Liu P, Cui LX, Meng Y, Tao SA, Han XZ, Sun BJ. Moderate climate warming scenarios during embryonic and post-embryonic stages benefit a cold-climate lizard. *Funct Ecol.* 2022:**36**(5): 1137–1150. https://doi.org/10.1111/1365-2435.14032.
- Lv P, Ma D, Gao S, Zhang Y, Bae YK, Liang G, Gao S, Choi JH, Kim CH, Wang L, et al. Generation of foxn1/Casper mutant zebrafish for allograft and xenograft of normal and malignant cells. Stem Cell Rep. 2020:15(3):749–760. https://doi.org/10.1016/j.stemcr. 2020.07.020.
- Ma Y, Bao J, Zhang Y, Li Z, Zhou X, Wan C, Huang L, Zhao Y, Han G, Xue T. Mammalian near-infrared image vision through injectable and self-powered retinal nanoantennae. *Cell.* 2019:**177**(2): 243–255.e15. https://doi.org/10.1016/j.cell.2019.01.038.
- Manceau M, Domingues VS, Linnen CR, Rosenblum EB, Hoekstra HE. Convergence in pigmentation at multiple levels: mutations, genes and function. *Philos Trans R Soc Lond B Biol Sci.* 2010:**365**(1552): 2439–2450. https://doi.org/10.1098/rstb.2010.0104.
- McNamara ME, Rossi V, Slater TS, Rogers CS, Ducrest AL, Dubey S, Roulin A. Decoding the evolution of melanin in vertebrates.

- Trends Ecol Evol. 2021:**36**(5):430–443. https://doi.org/10.1016/j.tree.2020.12.012.
- Morehouse NI, Vukusic P, Rutowski R. Pterin pigment granules are responsible for both broadband light scattering and wavelength selective absorption in the wing scales of pierid butterflies. *Proc R Soc B Biol Sci.* 2007:**274**(1608):359–366. https://doi.org/10.1098/rspb.2006.3730.
- Munguia P, Levinton JS, Silbiger NJ. Latitudinal differences in thermoregulatory color change in *Uca pugilator*. *J Exp Mar Biol Ecol*. 2013:**440**:8–14. https://doi.org/10.1016/j.jembe.2012.11.010.
- Noble DWA, Qi Y, Fu J. Species delineation using Bayesian model-based assignment tests: a case study using Chinese toad-headed agamas (genus *Phrynocephalus*). *BMC Evol Biol*. 2010:**10**(1):197. https://doi.org/10.1186/1471-2148-10-197.
- Orteu A, Jiggins CD. The genomics of coloration provides insights into adaptive evolution. *Nat Rev Genet*. 2020:**21**(8):461–475. https://doi.org/10.1038/s41576-020-0234-z.
- Ozeki H, Ito S, Wakamatsu K, Thody AJ. Spectrophotometric characterization of eumelanin and pheomelanin in hair. *Pigment Cell Res.* 1996:**9**(5):265–270. https://doi.org/10.1111/j.1600-0749. 1996.tb00116.x.
- Pan A, Saw WG, Subramanian Manimekalai MS, Gruber A, Joon S, Matsui T, Weiss TM, Gruber G. Structural features of NS3 of Dengue virus serotypes 2 and 4 in solution and insight into RNA binding and the inhibitory role of quercetin. Acta Crystallogr Sect D. 2017:73(5):402–419. https://doi.org/10.1107/S2059798317003849.
- Patterson N, Price AL, Reich D. Population structure and eigenanalysis. *PLoS Genet*. 2006:**2**(12):e190. https://doi.org/10.1371/journal.pgen.0020190.
- Pertea M, Kim D, Pertea GM, Leek JT, Salzberg SL. Transcript-level expression analysis of RNA-seq experiments with HISAT, StringTie and Ballgown. *Nat Protoc.* 2016:**11**(9):1650–1667. https://doi.org/10.1038/nprot.2016.095.
- Pinho C, Hey J. Divergence with gene flow: models and data. *Annu Rev Ecol Evol Syst.* 2010:**41**(1):215–230. https://doi.org/10.1146/annurev-ecolsys-102209-144644.
- Rausher MD, Delph LF. Commentary: when does understanding phenotypic evolution require identification of the underlying genes? *Evolution*. 2015:**69**(7):1655–1664. https://doi.org/10.1111/evo.12687.
- Robinson MD, McCarthy DJ, Smyth GK. EdgeR: a bioconductor package for differential expression analysis of digital gene expression data. *Bioinformatics*. 2010:**26**(1):139–140. https://doi.org/10.1093/bioinformatics/btp616.
- Rosenblum EB, Hickerson MJ, Moritz C. A multilocus perspective on colonization accompanied by selection and gene flow. *Evolution*. 2007:**61**(12):2971–2985. https://doi.org/10.1111/j.1558-5646.2007. 00251.x.
- Rosenblum EB, Hoekstra HE, Nachman MW. Adaptive reptile color variation and the evolution of the *Mc1r* gene. *Evolution*. 2004:**58**(8):1794–1808. https://doi.org/10.1111/j.0014-3820.2004.tb 00462 x
- Rosenblum EB, Römpler H, Schöneberg T, Hoekstra HE. Molecular and functional basis of phenotypic convergence in white lizards at White Sands. *Proc Natl Acad Sci USA*. 2010:**107**(5):2113–2117. https://doi.org/10.1073/pnas.0911042107.
- Sabeti PC, Varilly P, Fry B, Lohmueller J, Hostetter E, Cotsapas C, Xie X, Byrne EH, McCarroll SA, Gaudet R, et al. Genome-wide detection and characterization of positive selection in human populations. Nature. 2007:449(7164):913–918. https://doi.org/10.1038/nature06250.
- Semenov GA, Linck E, Enbody ED, Harris RB, Khaydarov DR, Alström P, Andersson L, Taylor SA. Asymmetric introgression reveals the genetic architecture of a plumage trait. *Nat Commun*. 2021:12(1):1019. https://doi.org/10.1038/s41467-021-21340-y.
- Sievers F, Wilm A, Dineen D, Gibson TJ, Karplus K, Li W, Lopez R, McWilliam H, Remmert M, Söding J, et al. Fast, scalable generation of high-quality protein multiple sequence alignments using

- Clustal Omega. *Mol Syst Biol*. 2011:**7**(1):539. https://doi.org/10. 1038/msb.2011.75.
- Smith KR, Cadena V, Endler JA, Kearney MR, Porter WP, Stuart-Fox D. Color change for thermoregulation versus camouflage in freeranging lizards. Am Nat. 2016:188(6):668–678. https://doi.org/10. 1086/688765.
- Solovyeva EN, Lebedev VS, Dunayev EA, Nazarov RA, Bannikova AA, Che J, Murphy RW, Poyarkov NA. Cenozoic aridization in Central Eurasia shaped diversification of toad-headed agamas (*Phrynocephalus*; Agamidae, Reptilia). *PeerJ.* 2018:**6**:e4543. https://doi.org/10.7717/peerj.4543.
- Stamatakis A. RAxML version 8: a tool for phylogenetic analysis and post-analysis of large phylogenies. *Bioinformatics*. 2014:**30**(9): 1312–1313. https://doi.org/10.1093/bioinformatics/btu033.
- Steiner CC, Rompler H, Boettger LM, Schoneberg T, Hoekstra HE. The genetic basis of phenotypic convergence in beach mice: similar pigment patterns but different genes. *Mol Biol Evol.* 2009:**26**(1):35–45. https://doi.org/10.1093/molbev/msn218.
- Steiner CC, Weber JN, Hoekstra HE. Adaptive variation in beach mice produced by two interacting pigmentation genes. *PLoS Biol.* 2007:**5**(9):e219. https://doi.org/10.1371/journal.pbio.0050219.
- Stevens M, Merilaita S. Defining disruptive coloration and distinguishing its functions. *Philos Trans R Soc Lond B Biol Sci.* 2009:**364**(1516): 481–488. https://doi.org/10.1098/rstb.2008.0216.
- Stevens M, Merilaita S. Animal camouflage. In: Stevens M, Merilaita S, editors. Animal camouflage: mechanisms and function. Cambridge: Cambridge University Press; 2011. p. 1–16.
- Stoddard MC, Eyster HN, Hogan BG, Morris DH, Soucy ER, Inouye DW. Wild hummingbirds discriminate nonspectral colors. *Proc Natl Acad Sci USA*. 2020:**117**(26):15112–15122. https://doi.org/10.1073/pnas.1919377117.
- Stuart-Fox D, Aulsebrook A, Rankin KJ, Dong CM, McLean CA. Convergence and divergence in lizard colour polymorphisms. *Biol Rev.* 2021:**96**(1):289–309. https://doi.org/10.1111/brv.12656.
- Stuart-Fox D, Moussalli A. Camouflage, communication and thermoregulation: lessons from colour changing organisms. *Philos Trans R Soc Lond B Biol Sci.* 2009:**364**(1516):463–470. https://doi.org/10.1098/rstb.2008.0254.
- Stuart-Fox D, Newton E, Clusella-Trullas S. Thermal consequences of colour and near-infrared reflectance. *Philos Trans R Soc Lond B Biol Sci.* 2017:**372**(1724):20160345. https://doi.org/10.1098/rstb. 2016.0345.
- Tao SA. Integration of morphological, behavioral, and physiological responses of toad-head amaga (Phrynocephalus putjatai) to thermal environments. Jinhua: Zhejing Normal University; 2022.
- Tao XQ, Jiang ZG, Ji SN, Chu HJ, Yang DD, Li CW. Influence of light intensity and substrate color on dorsal gray color change in Phrynocephalus helioscopus and Phrynocephalus grumgrzimailoi. J Arid Environ. 2018:157:22–26. https://doi.org/10.1016/j. jaridenv.2018.07.004.
- Tigano A, Friesen VL. Genomics of local adaptation with gene flow. *Mol Ecol.* 2016:**25**(10):2144–2164. https://doi.org/10.1111/mec. 13606.
- Townsend TM, Alegre RE, Kelley ST, Wiens JJ, Reeder TW. Rapid development of multiple nuclear loci for phylogenetic analysis using genomic resources: an example from squamate reptiles. *Mol Phylogenet Evol.* 2008:**47**(1):129–142. https://doi.org/10.1016/j.ympev.2008.01.008.
- Umbers KDL. Turn the temperature to turquoise: cues for colour change in the male chameleon grasshopper (*Kosciuscola tristis*) (Orthoptera: Acrididae). *J Insect Physiol*. 2011:**57**(9):1198–1204. https://doi.org/10.1016/j.jinsphys.2011.05.010.
- Utzeri VJ, Ribani A, Fontanesi L. A premature stop codon in the TYRP1 gene is associated with brown coat colour in the European rabbit (*Oryctolagus cuniculus*). *Anim Genet*. 2014:**45**(4):600–603. https://doi.org/10.1111/age.12171.
- Vroonen J, Vervust B, Fulgione D, Maselli V, Van Damme R. Physiological colour change in the Moorish gecko, *Tarentola mauritanica* (Squamata: Gekkonidae): effects of background,

- light, and temperature. *Biol J Linn Soc Lond*. 2012:**107**(1): 182–191. https://doi.org/10.1111/j.1095-8312.2012.01915.x.
- Weir BS, Cockerham CC. Estimating F-statistics for the analysis of population structure. *Evolution*. 1984:**38**(6):1358–1370. https://doi.org/10.1111/j.1558-5646.1984.tb05657.x.
- White NJ, Butlin RK. Multidimensional divergent selection, local adaptation, and speciation. *Evolution*. 2021:**75**(9):2167–2178. https://doi.org/10.1111/evo.14312.
- White TE, Kemp DJ. Technicolour deceit: a sensory basis for the study of colour-based lures. *Anim Behav*. 2015:**105**:231–243. https://doi.org/10.1016/j.anbehav.2015.04.025.
- Yang WZ, Feiner N, Laakkonen H, Sacchi R, Zuffi MAL, Scali S, While GM, Uller T. Spatial variation in gene flow across a hybrid zone reveals causes of reproductive isolation and asymmetric introgression in wall lizards. *Evolution*. 2020:**74**(7):1289–1300. https://doi.org/10.1111/evo.14001.
- Zhang Y. I-TASSER server for protein 3D structure prediction. BMC Bioinformatics. 2008:9(1):40. https://doi.org/10.1186/1471-2105-9-40.
- Zhu ZX, Jiang DL, Li BJ, Qin H, Meng ZN, Lin HR, Xia JH. Differential transcriptomic and metabolomic responses in the liver of Nile tilapia (*Oreochromis niloticus*) exposed to acute ammonia. *Mar Biotechnol*. 2019:21(4):488–502. https://doi.org/10.1007/s10126-019-09897-8.